Acoust. Sci. & Tech. **37**, 1 (2016)

TECHNICAL REPORT

Active wind noise hybrid control in motorcycle helmets

Demián García Violini[1,2,*], Ricardo S. Sánchez-Peña[1,3,†], Ariel Velis[4,‡] and Carlos Posse[4,§]

[1]*Buenos Aires Institute of Technology (Instituto Tecnológico de Buenos Aires), Av. Madero 399, CABA, Argentina*
[2]*National University of Quilmes, Roque Sáenz Peña 352, Bernal, Buenos Aires, Argentina*
[3]*National Council of Technical and Scientific Research (CONICET), Av. Rivadavia 1917, CABA, Argentina*
[4]*Acoustics and Lighting Laboratory (LAL), Cno. Centenario 505–508, M. B. Gonnet., Buenos Aires, Argentina*

(*Received 26 January 2015, Accepted for publication 10 April 2015*)

Abstract: In this work, three experiments are conducted. In a realistic environment (freeway), a database for the noise dynamics versus velocity in a motorcycle helmet is computed. Next, under the controlled conditions of an anechoic chamber, the models for the feedback (FB) and feedforward (FF) paths in the helmet are obtained by a filtering and identification process. Finally, in the same chamber, a hybrid (FB+FF) robust controller is tested against the actual noise measured in the freeway, and it achieves attenuations between 20 and 30 dB.

Keywords: Motorcycle helmets, Active noise control, H-infinity optimal control, Feedforward control, Hybrid control

PACS number: 43.50.Ki, 43.50.Hg, 43.50.Lj [doi:10.1250/ast.37.21]

1. INTRODUCTION

Active noise control (ANC) in motorcycle helmets has not been the most studied application since ANC entered the technological scene. Motorcyclists are exposed to high noise levels which affect their health and lead up to a condition known as noise-induced hearing loss (NIHL). There are a few works concerned with these health consequences in occupational motorcyclists [1–5]. In particular, policemen, delivery employees, sportsmen, are at risk of NIHL. Several medical studies point out that, with the inner helmet noise levels and the typical driving patterns, the percentage of exposed population that will suffer a hearing loss of 30 dB or more ranges from 40% for professional racers, 36% for paramedics and 6% for driving instructors.

This noise increases with speed and is generated by the interaction between the helmet and the surrounding air, mainly associated with turbulence effects [6,7]. Other noise sources, like the motorcycle's engine noise or the effect of the motorcycle tires on the asphalt are not significant above 65 km/h, and therefore are not considered here [8,9]. Based on the health recommendations, there are international standards which regulate the time length and noise dynamic exposure levels for working activities. These indicate a maximum tolerable level of 85 dB for an 8-hour workday [10–12].

Within this context, there are two methods to reach the recommended level: passive and active attenuation systems. The devices that seek to achieve passive reduction do not meet the present regulations [13]. In addition, such methods unfailingly remove critical information from the surrounding acoustical field (in some areas they are forbidden), and in general have low attenuation levels [8,14]. For example, the use of earplugs can be very practical, but it does not provide good attenuation for low-frequency noise, and it also complicates the use of radio communication equipment. The use of a neck seal has proven to reduce up to 4 dB at 120 km/h, but it can be difficult to fit in many situations and the wind can pull it out of the helmet [8,14]. In addition, the reduction of air flow within a helmet can lead to a buildup of CO_2 and heat, which could cause impaired cognitive performance [6].

On the other hand, active noise control (ANC) has been applied to many other problems, e.g. ventilation ducts,

*e-mail: ddgarcia@itba.edu.ar
†e-mail: rsanchez@itba.edu.ar
‡e-mail: arielvelis@yahoo.com
§e-mail: charlyposse@gmail.com

rooms, headphones, helmets, etc [15,16]. In 1997 [13] the use of noise-canceling earphones in full coverage style helmets was patented, and it proved that the use of ANC techniques does not present the disadvantages of passive ones. Nevertheless, there are very few ANC works on motorcycle helmets [6,7,13,17], probably due to the time-varying nature of the noise dynamics.

An important issue to be kept in mind is the adequate selection of the control structure [18–20]: feedback (FB), feedforward (FF), or its combination (FB+FF), also called *hybrid* active control. In addition, the knowledge of the noise level and dynamics as a function of speed is also important so as to design both active or passive sound attenuation devices. Previous works which offer this information have been presented in [6–8,14]. In [6] a study of the environmental noise on a moving motorcycle and a survey of users has been carried out. It gathers their opinion about the noise and the different attenuation methods. More than 95% of the respondents agree that a quieter helmet is necessary for their health and perception of the environment, and more than 92% answer that noise is too loud. In the survey, the relative wind velocity is not considered to asses the noise versus velocity curve and the plots have no scaling; hence there is no clear quantification of the noise control attenuation. In [7] a freeway experience has been conducted but with very few noise level and speed measurements, which at the same time are not precise enough. Besides, the dummy head used did not have an adequate design for an experience of this type. In [8,14] a velocity versus noise profile has been obtained in a wind tunnel, but with very few measurement points.

Consequently, the first part of the work presented here proposes a precise measurement of the wind noise level as a function of the relative air speed. To this end, several experiments were performed with a helmet mounted on a car roof and driven at different velocities in the freeway, in order to provide a realistic environment. A measurement database was generated which is useful for both active and passive noise attenuators used in realistic outdoor environments by motorcycle drivers. These measurements have been carried out on a head constructed specifically for this experience, and a helmet which has been instrumented with two different sensors.

Next, the experimental setup was moved to an anechoic chamber, where the physical system has been identified based on chin and ear microphones exposed to sinusoidal sound sweeps covering a practical frequency range obtained from the previous experiment. The models obtained were used to design robust FB and FF controllers in order to test the ANC closed loop. Finally, a performance test was carried out using a speaker which excites the helmet and head with the freeway noise obtained previously.

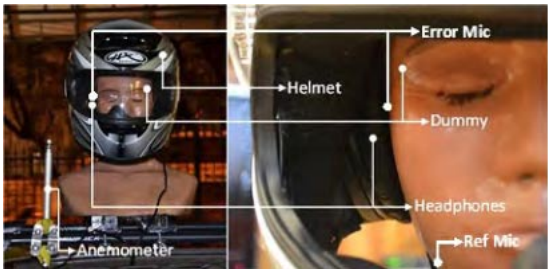

Fig. 1 Experimental setup on the car: head, anemometer, helmet and headphone.

Therefore, this work provides a precise measurement of the motorcycle noise dynamics, extending previous results [6–8,14]. In addition, a novel feedforward control strategy [21] is used in a practical ANC experiment, combined with a feedback controller, both based on the $\mathcal{H}_\infty$ norm minimization. The experimental ANC test performed with this hybrid controller in the anechoic chamber represents a *proof of concept* for active robust $\mathcal{H}_\infty$ hybrid control in motorcycle helmets. It is also a test for the maximum attenuation level that may be achieved before a real time experience can be performed in a street environment.

The paper is organized as follows. The experimental setup and instrumentation is described in in the following section, and freeway experiments and the resulting database are presented in Sect. 3. Sections 4 to 5.2. describe the experience inside the anechoic room, with both the identification and controller design and implementation, respectively. The paper ends with conclusion and future research directions in Sect. 6.

2. EXPERIMENTAL SETUP

A precise noise description in the motorcycle helmet and also an experimental proof of a novel active control algorithm are achieved here. Each stage of the experimental setup is described in what follows: the noise characterization stage on the freeway and the identification and control stages in the anechoic room.

The following hardware was used in both cases: a pair of Sennheiser HD 280 headphones placed inside the helmet, a dummy head specifically built for this purpose (Fig. 1), a couple of Knowles BT-21759 microphones without windscreen (Fig. 2) due to the absence of direct wind contact, and a National Instruments (NI) CompactRIO system (cRIO 9075 with a 9205 analog input card) for the data acquisition and real-time control.

For the freeway experience, a Testo 0628 0036 anemometer for the relative air speed measurement was used, together with an anti-vibration platform to mount the dummy on the car, and a 0.5 in. Brüel & Kjær model 4189 connected to a Sound Level Meter (SLM) of the same brand, model 2250.

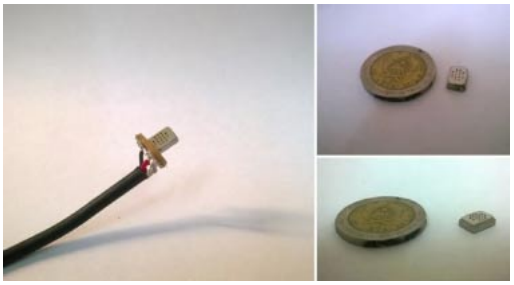

Fig. 2 Microphones.

In the anechoic chamber we also had an NI 9263 module for the analog output, and a JBL EON-315 speaker for the identification and control tests. The control was implemented on a Xilinx FPGA in the CompactRIO. A complete view of the experimental setup is shown in Figs. 1, 3, 4 and 9.

One of the Knowles microphones is located in one ear, more precisely in the pinna (error microphone). The other one is placed in the chin of the dummy head (reference microphone), see Fig. 10. These two microphones have adequate characteristics and size for this type of application. In addition, a Brüel & Kjær microphone was located in similar conditions in the other ear to have a more precise measurement for comparison. Due to the characteristic of this experiment, a random sound incidence excited the microphones, hence a correction of their frequency response was made a posteriori, since these models were for normal incidence. The output signal of the SLM was registered with the data acquisition system.

The Knowles microphone in the pinna is used to experimentally characterize the noise, and it is validated with the Brüel & Kjær sonometer. On the other hand, the Knowles chin microphone has an extra function: it works as the feedforward input for controller implementation.

This setup was placed in a car driven on the freeway at different velocities to obtain a useful noise-speed database which could be instrumental in active and/or passive noise attenuation (Fig. 4). This seems a practical solution to obtain this data. Some years ago, one of the authors performed measurements in a wind tunnel instead, but high velocities were difficult to achieve and the wind tunnel noise was very high as compared with the air turbulence inside the helmet, see [7].

The dummy head has been developed according to the regulations in [22,23]. The physical and anthropometric characteristics were taken into account, i.e. head density, bone structural transmission, skin elasticity and inter-aural transmission. One important component of this head are the ears. They were developed considering the standard dimensions of the *pinna* and the ear canal, their flexibility and elasticity. Figure 3 shows the dummy head used in all the tests.

Fig. 3 Dummy head construction.

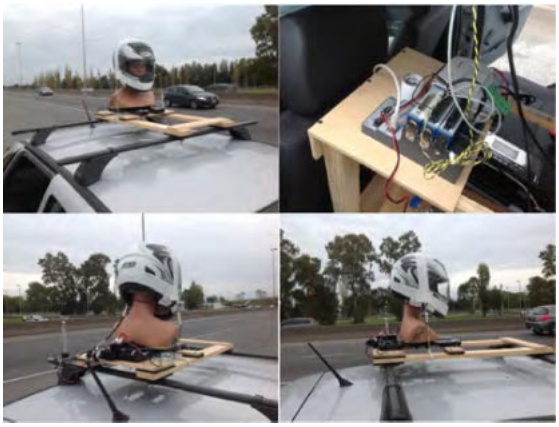

Fig. 4 Experimental setup on and inside the car during the freeway experience.

For the identification and control tests, the Knowles microphones (reference and error microphones), the electronic conditioning hardware, the acquisition and control hardware (CompactRio+FPGA) and the JBL external speaker were used. These experiments were carried out inside an anechoic chamber at the *Acoustics and Lighting Laboratory*.

3. FREEWAY EXPERIMENTS

This experiment was carried out by mounting the head with the instrumented helmet and the other hardware described in the previous section over a car roof, as illustrated in Fig. 4.

The sound pressure level L_{pF} measured by the SLM and the error microphone were obtained simultaneously with the velocity values from the anemometer. The value measured by the anemometer is the relative speed between the air and the helmet, which can be very irregular because of lateral winds and turbulence effects. In order to have a coherent and precise value of the speed and the sound level, an integration time of $T = 125\,\text{ms}$ was used. This assumes that the noise is approximately constant (in spectral terms) during this time interval. From the experi-

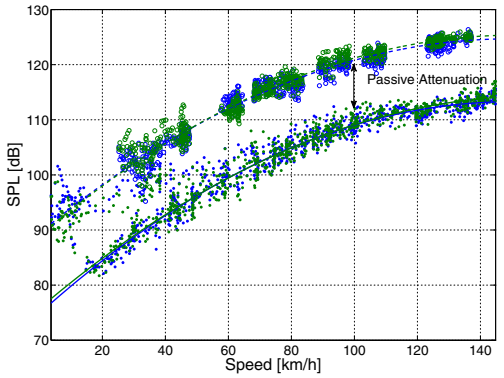

Fig. 5 Curve fit for sound pressure levels (dB) *vs.* speed. Empty and solid circles are the experimental data for the WoPA and WPA cases, respectively. The dashed and solid lines are the data interpolation for the WoPA and WPA cases, respectively. Blue and green distinguish between Brüel & Kjær and Knowles mics, respectively.

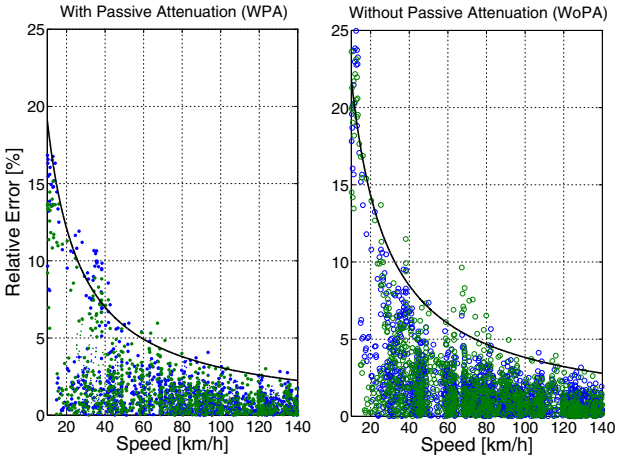

Fig. 6 Curve fit errors *vs.* speed with (WPA) and without (WoPA) the passive attenuation device. Here, 99% of the measurements are below the solid black line. Blue and green distinguish between Brüel & Kjær and Knowles mics, respectively.

ments, it has been verified that the speed does not suffer more than 1% variations with this integration time.

Based on the information provided by the manufacturer, it is assumed that the Brüel & Kjær has a flat frequency response. However, the frequency response of both microphones (Brüel & Kjær and Knowles) were also measured and verified inside the anechoic room. Thanks to this data the Knowles error microphone was compensated (off-line by software) to implement a flat response. As mentioned in Sect. 2, an additional compensation was made concerning the incidence correction, from normal to random.

With these compensations, the L_{pF} is estimated using the root mean square (RMS) value of the signals from the Brüel & Kjær sonometer and the additional Knowles microphone, as follows:

$$L_{pF} = 20\log_{10}\left[\frac{v_{\text{rms}}}{v_{\text{ref}}}\right] \quad \text{(dB)}$$

where v_{rms} represents the RMS voltage from each microphone and v_{ref} is the voltage reference value of their (flat) frequency response, which indicates a measure of their sensitivity. Finally, the calibration is completed using the experimental data for an optimal L_{pF} estimation, by correcting span and offset.

Two different experiments were proposed. The first one includes a passive attenuator which closes the gap between the helmet and the Dummy head (on the neck and below the chin) in order to reduce the incoming noise. The second experiment was conducted without this passive attenuation. Both cases are denoted as WPA (with passive attenuation) and WoPA (without passive attenuation), respectively.

The results of the estimation of the L_{pF} for both microphones are indicated in Fig. 5. With these experimental results, different interpolated models were proposed. Finally, an algebraic quadratic function fitted the L_{pF} as a function of speed as follows:

$$L_{p(est)} = p_1 v^2 + p_2 v + p_3 \quad \text{(dB)} \qquad (1)$$

which can be used from 20 to 145 km/h (see also comments at the end of this section). The relative estimation error and its dispersion level for both cases (WPA and WoPA) is indicated in Fig. 6. Note that the dispersion decreases with speed and that both microphone L_{pF} estimations have equivalent dispersion ranges, as indicated by blue and green points in the same figure. It can also be noted that above 60 km/h, the dispersion is lower than 5% in both cases.

Based on these results, the difference between the interpolated models can be considered to be the effect of the passive attenuator, which results in values between 12 and 14 dB. Taking into consideration that the overall level is above 105 dB for 100 km/h and faster, even in the WPA case, an active attenuation solution seems necessary to comply with the international labor regulations for 8-hour workdays [12].

In addition, the noise dynamics as a function of speed has been obtained, as indicated by the frequency response curves depicted in Fig. 7, in the WPA case. Furthermore, the power spectral density can be combined with an A-weight in order to obtain a result similar to the one in Fig. 5, but in dB(A). Again, by applying this process with the same time interval ($T = 125$ ms) used in the spectral analysis, a similar L_{pF} result can be derived in dB(A) and also a second degree polynomial fit. The results for each microphone in dB and dB(A) are indicated as L_{pF} and L_{pAF} respectively, for the WPA and WoPA cases in Table 1.

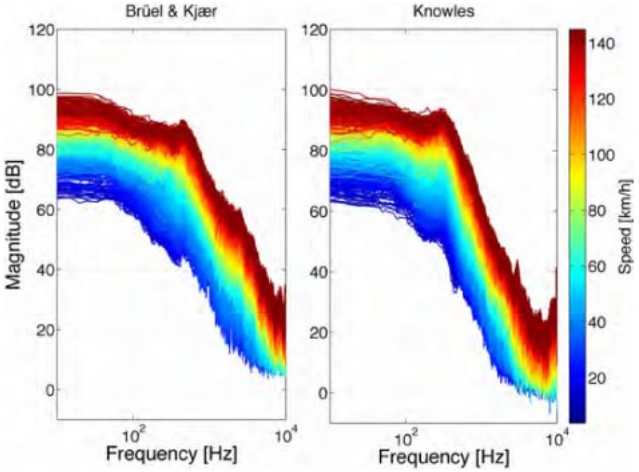

Fig. 7 Frequency response in dB measured by the Brüel & Kjær microphone (left), and the compensated Knowles microphone (right), parameterized by speed.

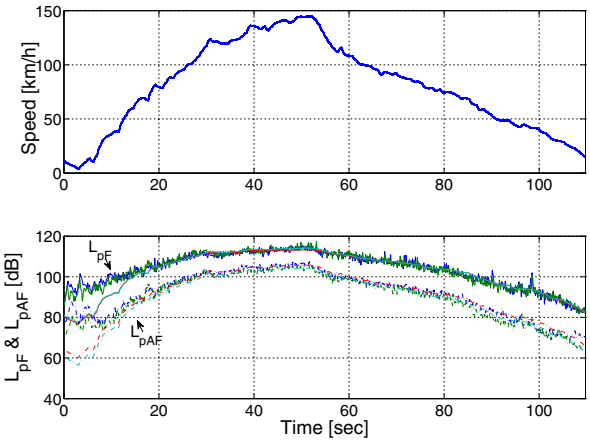

Fig. 8 Sound pressure levels (dB) integrated at $T = 125$ ms, for different speeds, in the WPA case. The solid line indicates L_{pF} and the dashed line L_{pAF}. The blue and green lines indicate the RMS estimations for the Brüel & Kjær and Knowles signals, respectively, while the red and cyan lines indicate the SPL estimations from the fitted curves.

Table 1 Sound levels in dB, measured with the Knowles at different velocities. The last row shows the relative error with respect to the Brüel & Kjær.

Speed (km/h)	WPA (L_{pF})	WPA (L_{pAF})	WoPA (L_{pF})	WoPA (L_{pAF})
40	92,8	75,8	105.7	89.3
50	96.3	80.3	109.1	94.8
60	99.4	84.4	112.1	99.6
70	102.3	88.1	114.9	103.9
80	104.9	91.4	117.3	107.5
90	107.1	94.4	119.4	110.5
100	109.1	97.1	121.2	112.9
110	110.7	99.3	122.7	114.7
120	112.1	101.2	123.8	115.8
130	113.1	102.7	124.7	116.4
140	113.8	103.9	125.2	116.3
Error	<0.65%	<3%	<0.5%	<1.1%

Table 2 Coefficient table for the algebraic data fit in each case.

Interpolation parameters	WPA (L_{pF})	WPA (L_{pAF})	WoPA (L_{pF})	WoPA (L_{pAF})
p_1 ($\times 10^{-3}$)	−1.54	−1.84	−1.59	−3.08
p_2	0.4874	0.6116	0.4816	0.8256
p_3	75.737	54.273	88.995	61.182

These are calculated by using the algebraic curve fit in each case according to Eq. (1). The last row of the table indicates the error obtained by comparing the Knowles L_{pF} estimation and the Brüel & Kjær, assuming that the actual value is defined by the latter. Table 2 presents the coefficients for the algebraic fitting in Eq. (1) in each case. Due to the fact that the human ear tends to a flat dynamic response in high level ranges ($L_{pF} > 110$ dB), the results are also presented in dB.

As a final verification, a particular speed profile is used to test the (L_{pF}, L_{pAF}) estimations. Considering the WPA case, the sound pressure level is estimated by means of two different methods. The first one is based on the RMS value for the Knowles and the Brüel & Kjær microphones. The second method uses the curve fit as a function of speed. In both cases (RMS and curve fit), the L_{pF} and speed curves are obtained by integrating again in intervals of 125 ms as indicated in Fig. 8. As a result, the speed and noise variations can be assumed to be almost constant during this time interval.

Note that at lower speeds, the fit has a poor adjustment. This can be attributed to the fact that below 60 km/h, the turbulence effect is not the main source of noise. As indicated in [8,9]: *...above about 65 km/h the wind noise generated by the airflow over a motorcycle and rider exceeds the noise from the motorcycle itself.* An in depth study of this effect would require a noiseless wind tunnel, but this is out of the scope of this work.

4. IDENTIFICATION EXPERIMENTS

4.1. Model Identification

A hybrid (FB+FF) linear time-invariant (LTI) control structure is used as indicated in Fig. 10, where G^{ff} represents the dynamics from the reference chin microphone of the Dummy head to the error microphone in the pinna. G^{fb} represents the dynamics from the input voltage in the headphones to the output signal of the error microphone. All the experiments were carried out inside an anechoic chamber (see Fig. 9). For the identification of G^{ff} an external speaker was used to excite both microphones, the reference one as the input and the error

Fig. 9 Experimental setup in the anechoic room.

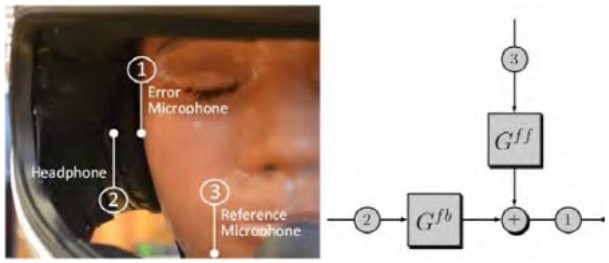

Fig. 10 Hybrid controller structure.

microphone signal as the output. On the other hand, in order to identify G^{fb}, the input voltage on the headphones was the input and the error microphone signal was the output. Both cases can be seen in Fig. 10.

These dynamics are represented by the *model set* $\mathcal{G}$ instead of a single model, which provides a more realistic representation of the actual behaviour. This set is described by using an additive uncertainty structure as follows

$$\mathcal{G} \triangleq \{G = G_0(s) + W_\Delta(s)\Delta,\ \Delta \in \mathbb{C},\ \|\Delta\| < 1\} \quad (2)$$

Here $G(s)$ must be read as $G^{ff}(s)$ or $G^{fb}(s)$ depending on each case, FF or FB. The nominal models are either $G_0^{ff}(s)$ or $G_0^{fb}(s)$. The weights $W_\Delta^{ff}(s)$ or $W_\Delta^{fb}(s)$ represent the uncertainty distribution as a function of frequency $s = j\omega$. Δ provides the model uncertainty set. Note that $\mathcal{G}$ includes an infinite number of models. Based on this description, a model identification methodology similar to the one in [24] is applied.

The identification experiments were performed using four different sinusoidal sweeps to excite the systems, which the proposed model set $\mathcal{G}$ should include. Each sweep had a frequency range of 20 Hz to 10 kHz. The data acquisition frequency was 40 kHz. A set of input/output data streams (u_i, y_i) were measured, where the index $i = 1, 2, 3, 4$ refers to the i-th sweep. With this data, a set of empirical transfer function estimated (ETFE) models were computed:

$$\hat{G}_i(j\omega_k) = \frac{Y_i(j\omega_k)}{U_i(j\omega_k)} + V_i(j\omega_k) \quad (3)$$

for $k = 1, \ldots, N$. Here $V_i(j\omega_k)$ is a stochastic process which reflects the differences in each experiment. In this framework, at each frequency w_k the estimated $\hat{G}_i(j\omega_k)$ is a random variable distributed around its mean value. To decrease the variance on each ETFE, a frequency Hamming window smoothing was applied following the guidelines established in [25]. With each smoothed ETFE a new data set is defined at each frequency ω_k as the center of the circle with minimum radius r_k, which contains all the smoothed ETFE ($i = 1, \ldots, 4$). From this new data set and using the *a priori* fact that the physical system is stable, a nominal model $G_0(s)$ is computed by using a subspace identification method [26,27]. The description in (2) includes all these circles, i.e. the radius centered around $G_0(j\omega_k)$ should satisfy $|W_\Delta(j\omega_k)\Delta| \geq r_k$ for all ω_k, $k = 1, \ldots, N$. Figure 11 shows the smoothed data (center of minimum radius circle, in red) and nominal models (in black) for the FF and FB systems.

The uncertainty level is computed by using the difference between the data points $\hat{G}(j\omega_k)$ and the nominal model $G_0(j\omega_k)$ as follows:

$$|W_\Delta(j\omega_k)| \geq \max_{1 \leq i \leq 4} \left| \frac{\hat{G}_i(j\omega_k) - G_0(j\omega_k)}{G_0(j\omega_k)} \right|, \quad \forall \omega_k$$

$k = 1, \ldots, N$. From here, the uncertainty weight $W_\Delta(s)$ is estimated. The magnitude of this weight covers the model uncertainty, i.e. the difference between model and data, at all discrete frequency points (ω_k, $k = 1, \ldots, N$) and for all four experiments. This guarantees that the controller will achieve robust stability, i.e. closed-loop stability for all models in set $\mathcal{G}$. Both nominal models G_0^{ff} and G_0^{fb} have order 8, and the uncertainty weights W_Δ^{ff} and W_Δ^{fb} have order 2.

5. CONTROL EXPERIMENTS

5.1. Control Design

The controller design has a hybrid structure (FF+FB), based on the $\mathcal{H}_\infty$ norm optimization. The $\mathcal{H}_\infty$ optimal controller used in the FB case is a standard tool in the robust control framework (see [28,29]). For the FF controller, the results in [21] have been applied. All the models obtained in the previous subsection (G_0^{ff}, G_0^{fb}, $W_\Delta^{ff}, W_\Delta^{fb}$) have been used.

Both controllers, FF and FB, can be designed independently and their combination achieves a better performance level than that of each separately (see [30]). Figure 12 indicates the structure used in the designs. In both cases, the information obtained from the noise characterization stage (Sect. 3) is also used to tune the controllers in terms of the attenuation band and level. The attenuation band is focused between 100 Hz and 300 Hz, because the audible sensitivity and the noise spectral density are larger there. To this end two performance weights were designed to

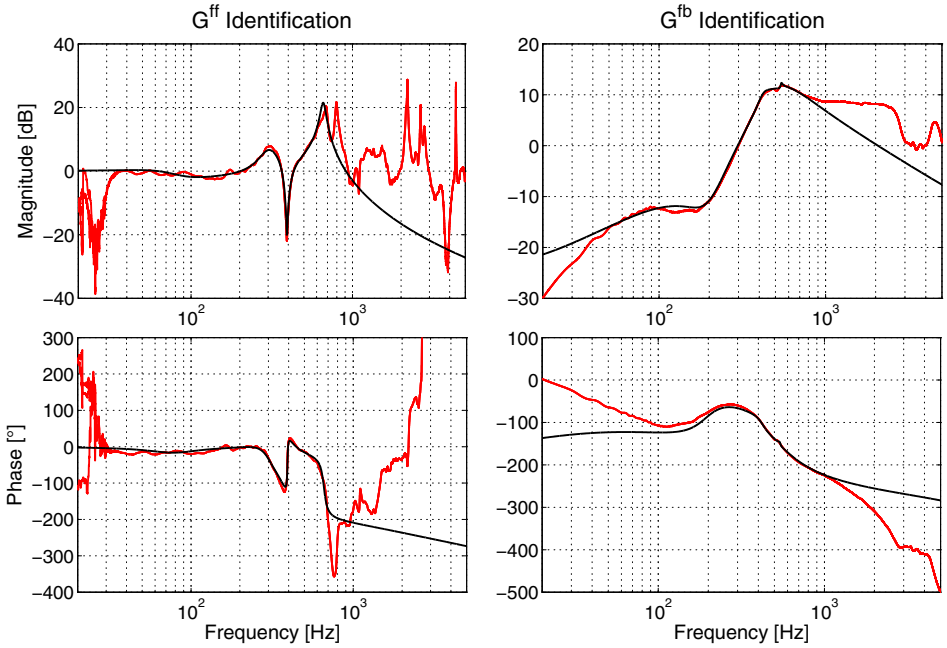

Fig. 11 Feedback and feedforward path identification. Nominal models (black) and smoothed data values (red).

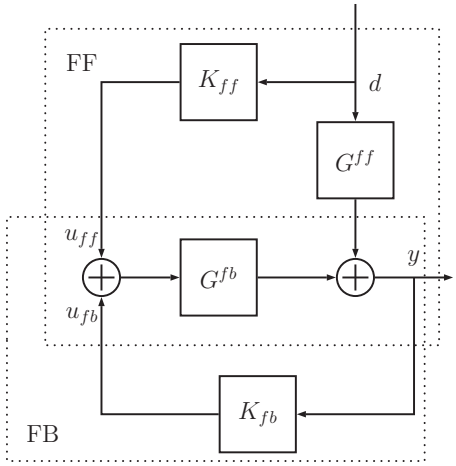

Fig. 12 Robust design procedure.

achieve this objective, W_p^{fb} and W_p^{ff} for the FB and FF cases, respectively.

5.1.1. Feedback controller design

The feedback controller design is based on the classical mixed sensitivity problem as described in [28,29]. It has been applied to the FB model in Fig. 12 and is defined as the stabilizing controller K_{fb}, which minimizes the following:

$$\min_{K_{fb}} \left\| \begin{bmatrix} (1 - S_{fb}) W_\Delta^{fb} \\ S_{fb} W_p^{fb} \end{bmatrix} \right\|_\infty$$

with $S_{fb} = (1 + G_0^{fb} K_{fb})^{-1}$.

5.1.2. Feedforward controller design

The feedforward design was also based on the $\mathcal{H}_\infty$ norm minimization. Two different methods were tested, [31] and [21]. The latter provided a better solution in terms of implementation and numerical issues.

In Fig. 12, unlike the feedback case, both systems, G^{ff} and G^{fb}, are taken into account in the design. The dynamic uncertainty is also a combination of both W_Δ^{ff} and W_Δ^{fb}. The aim here is to find a stable controller K_{ff} that solves the following optimization problem:

$$\min_{K_{ff}} \left\| \begin{bmatrix} 0 & 0 & W_\Delta^{ff} G_0^{ff} \\ 0 & 0 & K_{ff} W_\Delta^{ff} G_0^{fb} \\ W_p^{ff} & W_p^{ff} & W_p^{ff} (G_0^{ff} + G_0^{fb} K_{ff}) \end{bmatrix} \right\|_\infty$$

5.2. Controller Implementation

Both controllers K_{fb} and K_{ff} were designed as continuous time models and were implemented in discrete time. Therefore a discrete version of each one was obtained based on a bilinear (*Tustin*) discretization with a sample rate of 50 kHz. The controller orders were: 14 for K_{ff} and 12 for K_{fb}. In addition, robust stability and performance were guaranteed due to the fact that a model set was considered to represent model uncertainty [28,29].

For the controller implementation mentioned in Sect. 2, a National Instrument CompactRIO was used. The FPGA was programmed to run with a sampling rate of 50 kHz (for the controller discretization). To this end, a precise analysis of the magnitude of the frequency response was necessary in order to export the controller matrices in floating point to fixed point in 32bits.

The external speaker was used to reproduce the actual noise obtained in the freeway experiment described in

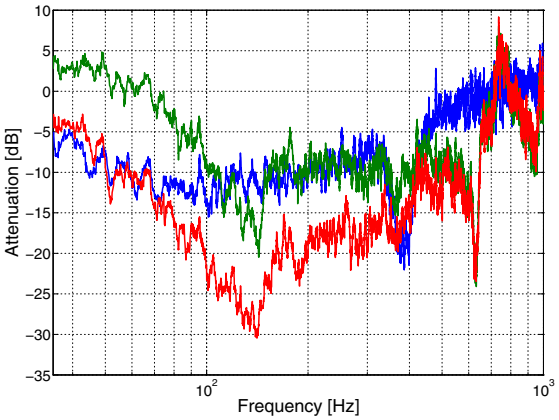

Fig. 13 Attenuation level for each control strategy: (blue) FB control, (green) FF control and (red) hybrid control.

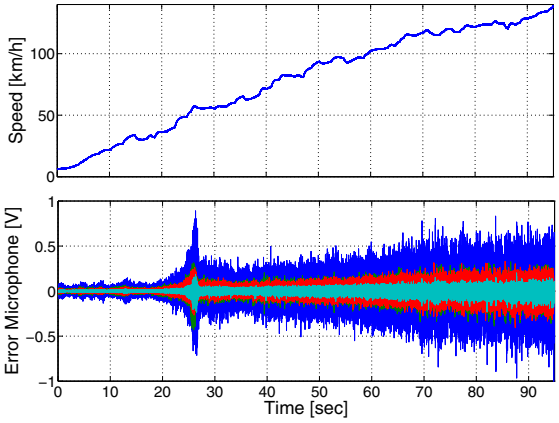

Fig. 14 Time response in freeway test for increasing velocity: (blue) Open loop noise, (green) FB control, (red) FF control and (cyan) hybrid control.

Sect. 3. This noise was obtained at different velocities, according to a certain profile. A different velocity profile from the one used in the model identification phase was selected, in order to have a better controller validation. According to Fig. 7, increasing speeds produce louder noise and higher frequency components. Therefore, in this experiment the noise impacting the helmet provides a physical representation of this particular velocity profile, which makes it more realistic.

The controller performance test was carried out inside the anechoic chamber using this noise to impact the head with the helmet (see Fig. 9). Figure 13 uses this actual experimental data and it shows the attenuation levels as a function of frequency. It can be highlighted that an attenuation peak level of 30 dB was achieved near 200 Hz. Besides, in the band $[100, 300]$ Hz, the same figure indicates attenuations above 20 dB. Also note, as indicated before, that the combination of both controllers, FB and FF, produces better results than that of each individually. This is in general not obvious due to the fact that they could cancel their control actions in certain frequency ranges in general. In Fig. 14 the time signals obtained in this experiment are depicted. Note again the effect of each controller and the combination of both.

6. CONCLUSION & FUTURE RESEARCH

Three experiments were performed under realistic (freeway) and environmentally controlled (anechoic chamber) conditions. They provide a database for the noise dynamics versus velocity, models for the FB and FF paths in the helmet through an identification process, and a performance test for a hybrid controller. The objective is to have a *proof of concept* for active noise control in motorcycle helmets.

This represents a necessary previous step before this controller can be tested in actual street conditions. The next stage will be to perform this test in real time on a freeway and to extend it to a Linear parameter varying (LPV) controller. A performance comparison between the LPV and LTI version presented here will also be conducted.

ACKNOWLEDGEMENTS

The authors acknowledge the valuable collaboration of Nilda Vechiatti and Horacio Bonti from LAL. The first two authors of this article were supported by the PRH Program No. 71 (PICT 290 and PFDT) of the Ministry of Science, Technology and Innovation of Argentina.

REFERENCES

[1] A. W. McCombe, J. Binnington and D. Nash, "Two solutions to the problem of noise exposure for motorcyclists," *Occup. Med.*, **44**, 239–242 (1994).
[2] C. Jordan, "Noise induced hearing loss in occupational motorcyclists," *J. Environ. Health Res.*, **3**, 373–382 (2004).
[3] B. Kirchner, E. Evenson, R. Dobie, P. Rabinowitz, R. K. James Crawford and W. Hudson, "Occupational noise-induced hearing loss," *ACOEM Guid. Statement*, **54**, 106–108 (2012).
[4] W. V. Moorhem, K. Sheperd, T. Magleby and G. Torian, "The effects of motorcycle helmets on hearing and the detection of warning signals," *J. Sound Vib.*, **77**, 39–49 (1981).
[5] A. W. McCombe, "Hearing loss in motorcyclists: Occupational and medicolegal aspects," *J. R. Soc. Med.*, **96**, 7–9 (2003).
[6] C. H. Brown and M. S. Gordon, "Motorcycle helmet noise and active noise reduction," *Open Acoust. J.*, No. 4, pp. 14–24 (2011).
[7] R. Castañe-Selga and R. S. Sánchez-Peña, "Active noise hybrid time-varying control for motocycle helmets," *IEEE Trans. Control Syst. Technol.*, **18**, 602–612 (2010).
[8] M. Lower, D. Hurst and A. Thomas, "Noise levels and noise reduction under motorcycle helmets," *Proceedings of the Institute of Acoustics*, pp. 979–982 (1994).
[9] M. Lower, D. Hurst, A. Claughton and A. Thomas, "Sources and levels of noise under motorcyclists' helmets" (1996). [Online]. Available: http://www.isvr.co.uk/at_work/m_cycle.htm (accessed 2015-11-17).
[10] The European Parliament and the Council of the European Union, "On the minimun health and safety requirement

regarding the exposure of workers to the risks arising from physical agents (noise)" (2003).

[11] American National Standards Institute, "Determination of occupational noise exposure and estimation of noise-induced hearing impairment," ANSI S3.44-1996 (1996).

[12] P. A. Niquette, "Noise exposure: Explanation of OSHA and NIOSH safe exposure limits and the importance of noise dosimetry," white paper, Ethymotic Research, Inc. (2002).

[13] J. J. Lazzeroni and M. K. Carevich, "Noise cancelling microphone for full coverage style helmets," United States Patent 5684880 (1997).

[14] M. Lower, D. Hurst, A. Claughton and A. Thomas, "Sources and levels of noise under motorcyclists' helmets," *Proceedings of Internoise '96*, Vol. 2 (1996).

[15] P. Nelson and S. Elliot, *Active Control of Sound* (Academic Press, London, 1991).

[16] S. Kuo and D. Morgan, *Active Noise Control Systems: Algorithms and DSP Implementations* (John Wiley & Sons, New York, 1995).

[17] L. Liu, S. M. Kuo and K. P. Raghuathan, "Active noise control for motocycle helmets," *Int. J. Inf. Commun. Eng.*, **6**, 102–107 (2010).

[18] J. Hong and D. Bernstein, "Bode integral constraints, colocation, and spillover in active noise and vibration control," *IEEE Trans. Control Syst. Technol.*, **6**, 111–120 (1998).

[19] M. Bai and D. Lee, "Comparison of active noise control structures in the presence of acoustical feedback by using the $\mathcal{H}_\infty$ synthesis technique," *J. Sound Vib.*, **206**, 453–471 (1997).

[20] R. S. Sánchez-Peña, J. Quevedo and V. Puig, Eds., *Identification and Control: The Gap between Theory and Practice* (Springer-Verlag, London, 2007), Chap. 8, pp. 203–244.

[21] A. Giusto and F. Paganini, "Robust synthesis of feedforward compensators," *IEEE Trans. Autom. Control*, **44**, 1578–1582 (1999).

[22] IEC, *International standards concerning electroacoustic measurements* (*Provisional head and torso simulator for acoustic measurements on air conduction hearing aids*), IEC/TR 60959 (1990).

[23] A. Vistosi, "Desarrollo de un sistema de medición para la obtención de la HRTF de un HATS," Master's thesis, Facultad de Ingeniería, U.B.A. (2009).

[24] D. García Violini, R. S. Sánchez-Peña and A. Velis, "Time-varying noise control in motorcycle helmets," *Acoust. Sci. & Tech.*, **36**, 333–335 (2015).

[25] L. Ljung, *System Identification — Theory For the User* (Prentice-Hall, Upper Saddle River, N.J., 1999).

[26] P. Van Overschee and B. De Moor, "N4SID: Subspace algorithms for the identification of combined deterministic and stochastic systems," *Automatica*, **30**, 7345 (1994).

[27] M. Verhaegen, "Identification of the deterministic part of MIMO state space models given in innovations form from inputoutput data," *Automatica*, **30**, 6174 (1994).

[28] R. S. Sánchez-Peña and M. Sznaier, *Robust Systems Theory and Applications* (John Wiley & Sons, New York, 1998).

[29] K. Zhou, J. C. Doyle and K. Glover, *Robust and Optimal Control* (Prentice-Hall, Upper Saddle River, N.J., 1996).

[30] S. Devasia, "Should model-based inverse inputs be used as feedforward under plant uncertainty?" *IEEE Trans. Autom. Control*, **47**, 1865–1871 (2002).

[31] G. Scorletti and V. Fromion, "Further results on the design of robust $\mathcal{H}_\infty$ feedforward controllers and filters," *2006 Conference on Decision and Control*, pp. 3560–3565 (2006).